Supplementary Information

Nitrogen-doped reduced graphene oxide electrodes for electrochemical supercapacitors

Spray Deposition

N-rGO was spray-deposited on ITO/glass substrates using a Prism Ultracoat 300 spray tool. Dispersions of N-rGO (~0.5 mg ml^{-1}) in water were prepared by tip-sonicating for 1 hour prior to loading into the spray tool. The spray tip was maintained at a distance of 35 mm from the substrates throughout the process with the substrates heated to 100 °C. A flow of 1 ml min^{-1} was used throughout with an air pressure of ~69 kPa following a standard spray pattern over an area of 9x6 cm^2.

X-ray Photoelectron Spectroscopy Analysis

N-rGO was mounted for XPS measurements by pressing the powder in to indium foil prior to loading into the equipment. This ensured that any contributions from the substrate are distinct from those of the sample and may be ignored. Comparing the survey spectra of GO and N-rGO in fig.1 (a) of the main text it is clear that the oxygen characteristic O1s peak (found at ~532 eV) is diminished after the plasma treatment. The ratio of carbon to oxygen (C/O ratio) for N-rGO is increased to 6.3, compared to that of GO, 2.2, after treatment; signifying the removal of oxygen species from the material. Of note is the presence of the nitrogen characteristic N1s peak at ~400 eV in the N-rGO, corresponding to a nitrogen doping level of 4.6%. The indium 3d characteristic peaks visible in the GO survey spectrum are a result of sample mounting and do not affect the interpretation of the carbon and oxygen peaks. The characteristic C1s peaks (found at ~284 eV) of the GO and N-rGO were subjected to further scrutiny in order to ascertain the nature of the functionalisation in each material. Spectral contributions were fitted to the measured spectra and these are displayed in fig.1 (b) and (c) of the main text. It should be noted that the GO sample was electrically insulating so a charge compensation process was employed which often overcompensates and shifts peaks to lower binding energies than expected. The conductive N-rGO did not require such a technique.

The major feature of the C1s peak in these samples is a peak corresponding to graphitic or sp^2-hybridised carbon at ~284.5 eV.[1,2] Functional groups are seen as a shoulder region on this peak at slightly higher binding energies. For GO, this shoulder is found to be, in fact, of higher intensity than the graphitic peak and the entire C1s region takes the form of a doublet. This is illustrative of the heavily oxygen functionalised nature of the material. After plasma treatment this doublet shape is changed to that of a primary peak with a significant shoulder. A peak corresponding to carbon in sp^3 configuration, at ~285.5 eV,[2] was found to significantly reduce in intensity relative to the graphitic peak during the reduction/doping process; this is indicative of partial restoration of the graphitic structure. The peaks corresponding to oxygen functional groups are all seen to reduce significantly in intensity after plasma treatment. Hydroxyl groups form a peak at ~286.7 eV,[3–5] carbonyl groups at ~288.2 eV[2,3] and carboxyl groups are seen at ~289.3 eV.[6] After the plasma treatment, two new peaks are visible in the C1s region. These correspond to nitrogen functional groups in sp^2 (~286.1 eV) and sp^3 (~287.3 eV) configurations. Also visible in the N-rGO C1s region is a shoulder at ~283 eV. This is attributed to sample preparation and mounting and may be disregarded when considering the nature of oxygen or nitrogen functional groups in the sample. Applying similar peak fitting procedures to the N1s peak of the N-rGO allows the nature of the nitrogen functionalisation to be quantified; this is shown in Fig. 1 (d) in the main text. The nitrogen moieties in the N-rGO were found to comprise pyridinic, pyrrolic and quaternary configurations (peaks found at ~399, ~400.1 and ~401.3 eV, respectively).[4,7] A small amount of nitrogen was also found to be present in the form of amine functional groups and manifested as a peak at ~397.5 eV.[8,9]

X-Ray Diffraction

Powder X-Ray Diffraction (XRD) was performed on the materials used in this study and their diffraction patterns were compared, as shown below in fig. S1. Also included is a comparison with graphite powder. The GO displays a diffraction peak at 2θ=12.3°, indicating an interplanar spacing typical of GO.[10] The N-rGO diffraction pattern also has a strong peak at this position, with no recovery towards the peak position of graphite, as would typically be expected for rGO. This indicates that the layer spacing for N-rGO is similar to that of the GO and is due to the fact that the N-rGO is still rather heavily functionalised, despite the reduction in oxygen content.
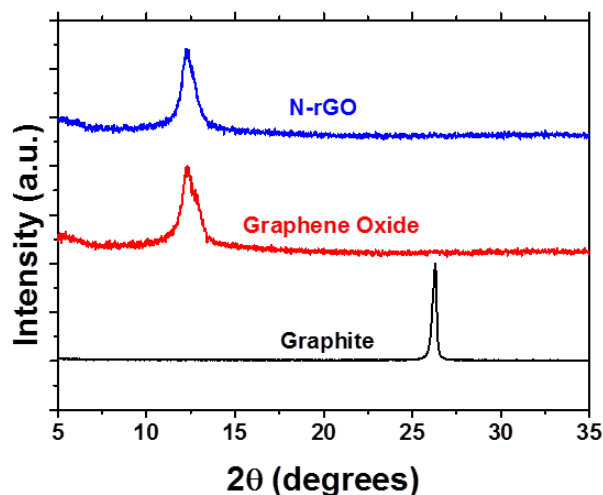
Figure S1: X-Ray diffraction pattern for graphite, GO and N-rGO.

Brunauer–Emmett–Teller Analysis

Brunauer–Emmett–Teller (BET) analysis was performed on GO and N-rGO powder to determine their specific surface areas. It was found that the GO displayed a surface area of 59 m^2 g^{-1} while the surface area of the N-rGO was 63 m^2 g^{-1}. These values should be treated with some caution when considering the supercapacitor electrodes. Electrode fabrication involved the aqueous dispersion of the materials via tip-sonication followed by spray deposition on to the electrode substrates. This processing is likely to cause the effective specific surface area of the material to change and, thus, the values determined by BET are not immediately relevant to the performance of the electrodes.

Electrochemical Comparison to Graphene Oxide (GO)

Electrodes were fabricated from GO using the same technique as was used for N-rGO. Electrochemical measurements indicated a significant improvement in the performance of the plasma treated N-rGO compared to the untreated GO. The GO electrodes displayed behaviour somewhat similar to the N-rGO insofar as the specific capacitance increased with cycle number. However, the capacitance was significantly lower than that for N-rGO and ultimately the electrode failed before any stable performance was reached. This is illustrated in fig. S2, below. It was found that the spray-deposited GO film delaminated from the ITO substrate over the course of the measurements as the electrode material failed. This was not observed on the N-rGO samples for the same measurements. It was deduced that the GO film undergoes redox processes which are irreversible over time and ultimately causes the film to delaminate. This is shown in fig. S2 (a) where initially redox peaks emerge with increasing cycle number but after a time these peaks disappear from the voltammogram as the film fails and ultimately the capacitance drops dramatically. The failure of the electrode can clearly be seen in fig. S1 (b). Voltammetric responses in fig. S2 (a) taken after this electrode failure are presented in red to indicate the disappearance of the redox behaviour and ultimately the drop in specific capacitance.
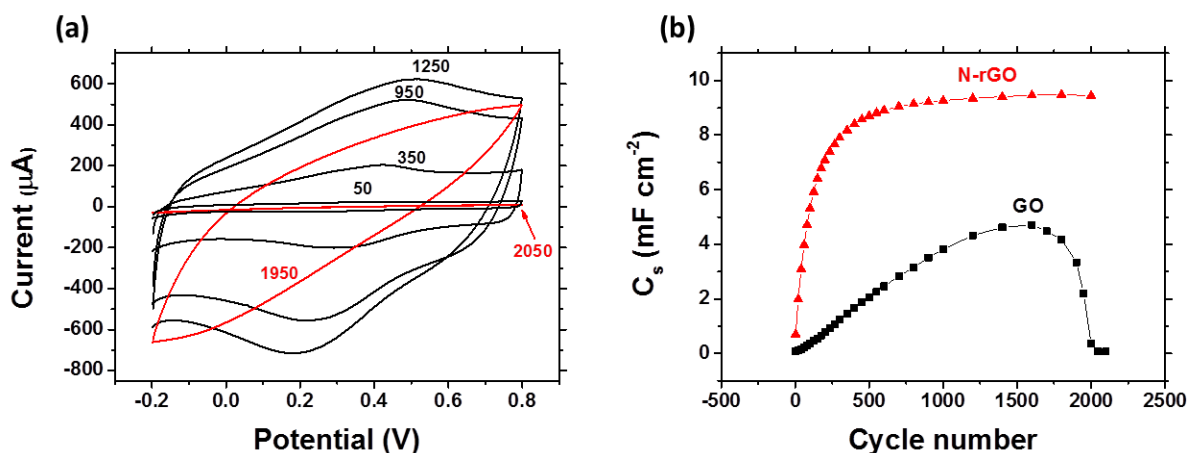
Figure S2: (a) Voltammograms for repeated cycling of GO working electrode in 1 M H_2SO_4 electrolyte at a scan rate of 100 mV s^{-1}. Cycle number corresponding to each voltammogram is indicated. Those voltammograms taken after the electrode fails are indicated in red. (b) Comparison of surface specific capacitance versus cycle number for N-rGO (red) and GO (black).

Further Electrochemical Measurements

Galvanostatic charge/discharge measurements

In addition to the cyclic voltammetry measurements presented in the main body of the text, galvanostatic Cyclic Charge/Discharge (CCD) measurements were carried out using the three electrode configuration in 1 M H_2SO_4. A constant charging/discharging current of 2 mA was applied and an example of a typical charge/discharge curve is shown in fig. S3. An IR drop due to internal resistance of the set-up is visible. The capacitance of the electrode for galvanostatic CCD measurements was calculated from the discharge portion of the curve in fig. S3 by the following formula, as detailed by Stoller and Ruof.[11]

$$C = I \bigg/ \frac{dV}{dt} \tag{S1}$$

C represents the capacitance of the electrode, I is the constant discharge current and dV/dt is the slope of the discharge portion of the CCD curve. Based upon this, a specific capacitance of ~8.9 mF cm^{-2} was calculated for the N-rGO electrode as measured by galvanostatic CCD. This is very similar to that calculated from cyclic voltammetry data in the main text, corroborating the conclusions drawn from that data. Also of note is the non-linearity of the CCD curves. Non-faradaic processes will display purely linear charge/discharge behaviour, but electrodes with pseudocapacitive character will deviate from this.[11] This is consistent with the findings of the three electrode cyclic voltammetry results where a significant amount of surface faradaic processes were observed to occur.
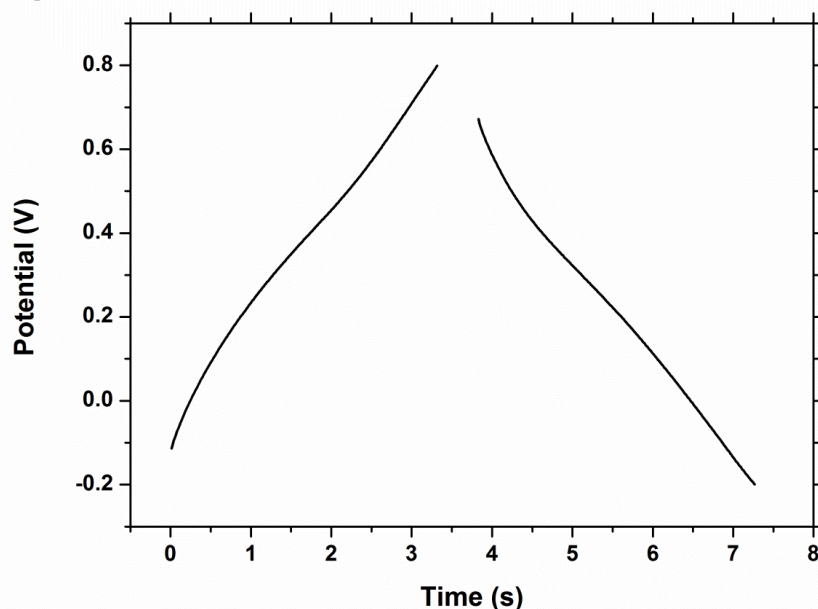
Figure S3: Constant current charge/discharge curve for N-rGO in 1 M H_2SO_4, charging current of 2 mA.

Other electrolyte systems

Further cyclic voltammetry was performed on N-rGO electrodes in 1 M KOH electrolyte to investigate further, non-acidic, aqueous electrolyte systems. A typical voltammogram is shown below in fig. S4. Of note is the lack of redox peaks when compared to the measurements performed in acidic media. Consequently, the charging currents are significantly smaller than for H_2SO_4 electrolyte given the absence of a pseudocapacitive contribution. The voltammetric profile shown here was typical of all scans across thousands of cycles. Unlike the data presented in the main text, there was no initial period of cycling for reversible behaviour to be established as there were no faradaic processes occurring at the electrode surface in the basic electrolyte. Hence, no "settling in" period was required for these redox processes to become established and fully reversible.
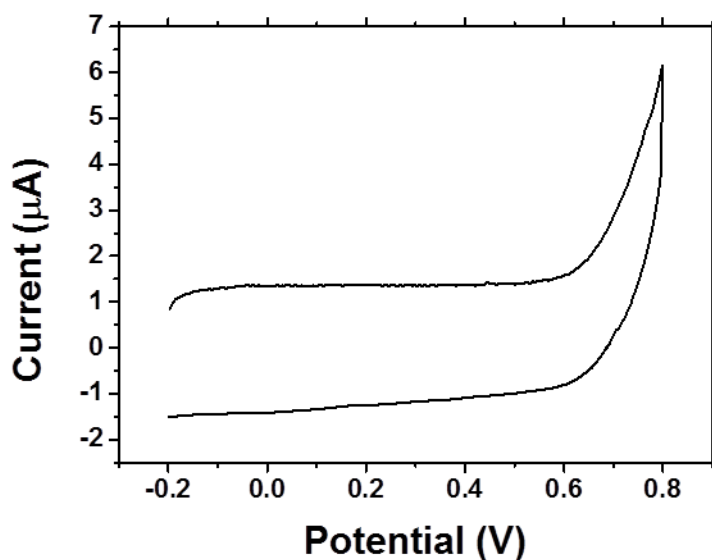
Figure S4: Cyclic voltammogram for N-rGO electrode in 1 M KOH.

References

1. X. Mei and J. Ouyang, *Carbon*, 2011, **49**, 5389–5397.
2. H. L. Poh, F. Šaněk, A. Ambrosi, G. Zhao, Z. Sofer, and M. Pumera, *Nanoscale*, 2012, **4**, 3515.
3. H. Wang, T. Maiyalagan, and X. Wang, *ACS Catal.*, 2012, **2**, 781–794.
4. O. C. Compton, D. A. Dikin, K. W. Putz, L. C. Brinson, and S. T. Nguyen, *Adv. Mater.*, 2010, **22**, 892–896.
5. D. Sun, X. Yan, J. Lang, and Q. Xue, *J. Power Sources*, 2013, **222**, 52–58.
6. Y. Wang, Y. Shao, D. W. Matson, J. Li, and Y. Lin, *ACS Nano*, 2010, **4**, 1790–1798.
7. Y.-C. Lin, C.-Y. Lin, and P.-W. Chiu, *Appl. Phys. Lett.*, 2010, **96**, 133110–133110–3.
8. B. Ruelle, S. Peeterbroeck, R. Gouttebaron, T. Godfroid, F. Monteverde, J.-P. Dauchot, M. Alexandre, M. Hecq, and P. Dubois, *J. Mater. Chem.*, 2006, **17**, 157–159.
9. J. Kim, D. Jung, Y. Park, Y. Kim, D. W. Moon, and T. G. Lee, *Appl. Surf. Sci.*, 2007, **253**, 4112–4118.
10. N. A. Kumar, H.-J. Choi, Y. R. Shin, D. W. Chang, L. Dai, and J.-B. Baek, *ACS Nano*, 2012, **6**, 1715–1723.
11. M. D. Stoller and R. S. Ruoff, *Energy Environ. Sci.*, 2010, **3**, 1294.